Clays Clay Miner., Vol. 70, No. 4:514–526, 2022
https://doi.org/10.1007/s42860-022-00199-0

ORIGINAL PAPER

Synthesis of Magnetic Sulfonated Carbon/Fe_3O_4/Palygorskite Composites and Application as a Solid Acid Catalyst

Mei Wu · Xingjun Yao · Jinlong Jiang · Yingnian Ji · Yaxi Gu · Qiulin Deng · Jing Ouyang

Accepted: 10 August 2022 / Published online: 6 September 2022
© The Author(s), under exclusive licence to The Clay Minerals Society 2022

Abstract Sulfonated carbon is a green, solid acid catalyst but its surface area, separation, and recovery after utilization need to be improved. The objective of the present study was to provide an environmentally friendly and economical method to prepare magnetic sulfonated carbon composite catalyst with a large surface area using palygorskite (Plg) as the support. A magnetic sulfonated carbon/Fe_3O_4/Plg composite catalyst was prepared via simultaneous calcination and sulfonation of the mixture of source, *p*-toluenesulfonic acid (TsOH), and Fe_3O_4/Plg. Fe_3O_4 nanoparticles and Plg nanorods were encased by a carbon layer derived from sucrose and TsOH. The composite catalyst exhibited good magnetic properties and high catalytic performance for the esterification of oleic acid with methanol. Oleic acid conversion reached 88.69% after the first catalytic cycle. Plg nanorods replaced sucrose and increased the catalyst's surface area. The introduction of Fe_3O_4 nanoparticles improved further the acid content and oleic-acid conversion and achieved 70.31% after five cycles. The catalyst was recycled easily using an external magnetic field and its magnetic property remained unchanged due to the protection of the carbon layer.

Keywords Esterification · Magnetic · Palygorskite · Solid acid catalyst · Sulfonated carbon

Associate Editor: Hongping He

M. Wu · J. Jiang (✉) · Y. Ji · Y. Gu
Faculty of Chemical Engineering, Key Laboratory for Palygorskite Science and Applied Technology of Jiangsu Province, Huaiyin Institute of Technology, Huai'an 223003, China
e-mail: jiangjinlong75@163.com

X. Yao
School of Chemistry and Chemical Engineering, Liaocheng University, Liaocheng 252059, China

Q. Deng
School of Materials Science and Engineering, Southwest University of Science and Technology, Mianyang 621010, China

J. Ouyang
National & Local Joint Engineering Research Center for Mineral Salt Deep Utilization, Huaiyin Institute of Technology, Huai'an 223003, China

Introduction

Solid acid catalysts have been applied to acid-catalyzed reactions as a replacement for liquid acid catalysts due to their easy recyclability, low corrosivity, and small degree of environmental pollution (Palani & Pandurangan, 2005; Sejidov et al., 2005; Testa et al., 2010; Pileidis et al., 2014). Sulfonated carbon catalyst is a novel solid acid catalyst derived from biomaterials and their products (Ngaosuwan et al., 2016; Toda et al., 2005). Sulfonated carbon catalysts exhibit high catalytic performance owing to their high acid density and good lipophilicity (Ballotin et al., 2020; Shu et al., 2010). However, their catalytic activities are often limited due to small surface area (Dehkhoda et al., 2010; Rao et al., 2011). Hence, the introduction of a porous structure to the interiors of sulfonated carbon materials (Konwar et al., 2014) or the

https://doi.org/10.1007/s42860-022-00199-0 Published online by Cambridge University Press

loading of sulfonated carbon materials on the surface of porous materials (Van de Vyver et al., 2010) can increase the catalyst's surface area, resulting in better catalytic performance. The preparation of sulfonated carbon catalysts often requires concentrated sulfuric acid as the sulfonation agent, which causes larger quantities of wastewater and consequently environmental pollution (Konwar et al., 2014). Sulfonated carbon catalysts have also been prepared by simultaneous carbonization-sulfonation of glucose and *p*-toluenesulfonic acid (TsOH) (Wang et al., 2011). Reports described this approach as simple and eco-friendly, where TsOH replaces concentrated sulfuric acid. The sulfonated carbon catalyst exhibits excellent catalytic performance in the dehydration of fructose into 5-hydroxymethylfurfural for high acid density.

In addition, sulfonated carbon catalysts with a small particle size were used to enhance the catalytic performance of a liquid-phase reaction system (Ngaosuwan et al., 2016; Shu et al., 2010). The separation and recovery of the catalysts from the liquid phase remain a challenge, therefore. The magnetic separation technique has been utilized to separate nanocatalysts effectively from the liquid phase (Mansoori & Mansoori, 2018; Polshettiwar et al., 2011). Magnetic heterogeneous catalysts also exhibit high catalytic activity and stability for the esterification reaction (Xie et al., 2018; Xie & Wang, 2021). Magnetic materials, such as Fe_3O_4 and Fe nanoparticles, were introduced into sulfonated carbon catalysts by loading and encapsulation (Kasprzak et al., 2018; Wang et al., 2019; Yang et al., 2020). The resulting sulfonated carbon catalysts inherited good magnetic properties from magnetic materials and also retained good catalytic performance.

Palygorskite (Plg) is a natural clay mineral that has been used as a functional carrier, such as for magnetic materials and carbon, due to its porous structure and nanofibrous morphology (Middea et al., 2015; Murray, 2000; Sarkar et al., 2015). Sulfonated carbon was loaded onto the surface of Plg nanorods via carbonization of sucrose, followed by sulfonation using concentrated sulfuric acid as the sulfonating agent. The resulting composite exhibited high catalytic performance for the synthesis of *n*-butyl acetate (Jiang, Xu, et al., 2012b). Recently, sulfonated carbon/Plg has been synthesized (via one-step carbonization-sulfonation using Plg as the support, sucrose as the carbon source, and TsOH as the sulfonating agent) and exhibited high catalytic performance for the esterification of oleic acid with methanol (Zhang et al., 2021). Furthermore, magnetic carbon/Plg composites have been prepared via hydrothermal treatment or impregnation-reduction (Tang et al., 2017; Zhang et al., 2020). The composite magnetic nanoparticles were well dispersed on the surface of rod-shaped Plg carriers. In addition, the magnetic carbon/Plg composite not only had good magnetic properties but also had significant adsorption capacities for pollutants.

The current study aimed to develop an environmentally friendly and economical preparation method of magnetic sulfonated carbon/Fe_3O_4/Plg composite catalyst, while obtaining the catalyst by the simultaneous calcination and sulfonation of the mixture of Fe_3O_4/Plg, TsOH, and sucrose. A further objective was to investigate the catalytic performance, magnetic property, and recyclability of the catalyst.

Materials and Methods

Materials

Plg from Gaojiawa (Xuyi, Jiangsu Province, China) was used. The sucrose, $FeSO_4{\cdot}7H_2O$, and NaCl were supplied by Tianjin Kemiou Chemical Reagent Co., Ltd., (Tianjin, China). TsOH and NaOH were purchased from Nanjing Chemical Reagent Co., Ltd., (Nanjing, China). The methanol, oleic acid, $FeCl_3{\cdot}6H_2O$, and HNO_3 were provided by Sinopharm Chemical Reagent Co., Ltd., (Shanghai, China). All reagents were of analytical grade and used directly without further purification.

Materials Preparation

Plg was milled using a ball grinder and then treated with HNO_3 solution (5 wt.%) for 24 h under magnetic stirring. The Plg obtained was centrifuged, washed with distilled water, and then dried at 80°C in an oven. Subsequently, pretreated Plg (5 g) was added to 100 mL of H_2O and ultrasonicated for 20 min. The mixture was added to 4.56 g of $FeSO_4{\cdot}7H_2O$ and 0.8 g of $FeCl_3{\cdot}6H_2O$ and stirred at 75°C for 10 min. The pH value of the mixture was adjusted to 12 using 1 mol/L NaOH solution. The magnetic Fe_3O_4/Plg composite was obtained after filtering, rinsing, and drying the solid precipitate.

The Fe_3O_4/Plg composite (5 g) was added to a solution composed of 15 mL of H_2O, 5 g of sucrose, and 1 g of TsOH. The mixture was stirred at room temperature for 1 h and dried under vacuum at 40°C. The dried solid

https://doi.org/10.1007/s42860-022-00199-0 Published online by Cambridge University Press

was milled in a ceramic mortar and then transferred to alumina combustion, which was placed in a horizontal tube furnace and heated at 200°C for 3 h under an N_2 atmosphere. The product was labeled SC-F-Plg-*n*, where *n* denotes the mass of the added sucrose, such as SC-F-Plg-1, SC-F-Plg-3, SC-F-Plg-5, and SC-F-Plg-7 at sucrose dosages of 1, 3, 5, and 7 g, respectively. As contrasting samples, sulfonated carbon/Plg (SC-Plg) and sulfonated carbon (SC) were prepared from a mixture of sucrose and TsOH under the same conditions with/without Plg, respectively.

Characterization

The sample morphologies were obtained using an S-3000N scanning electron microscope (Hitachi Corporation, Tokyo, Japan). The X-ray diffraction (XRD) patterns of the samples were recorded using a D8 Advance X-ray powder diffractometer (Bruker AXS, Karlsruhe, Germany) with CuKα radiation from 5 to 80°2θ at a scanning rate of 2°2θ/min. Transmission electron microscope (TEM) images and the corresponding TEM-EDS mapping were performed using a JEM 2100F transmission electronic microscope (JEOL Corporation, Tokyo, Japan) operating at 200 kV. Fourier-transform infrared (FTIR) spectra were recorded using a ThermoFisher Nicolet 5700 spectrometer (ThermoFisher Nicolet Corporation, Waltham, Massachusetts, USA). Elemental analysis of the catalysts was performed using an energy-dispersive X-ray spectrometer (EDX, EX-250, Horiba Corporation, Kyoto, Japan) and Elementar Vario EL III element analyzer (Elementar Corporation, Hannah, Germany), respectively. N_2 adsorption isotherms of the catalysts were obtained using a Micromeritics TriStar II 3020 apparatus (Micromeritics Instruments Corporation, Norcross, Georgia, USA) at –196°C (77 K). Before each measurement, the samples were degassed for 12 h at 150°C under N_2 atmosphere. The magnetic properties of the magnetic samples were determined using a superconducting quantum interference device (SQUID, Quantum Design, San Diego, California, USA). Chemical analyses of samples were determined using an X-ray fluorescence (XRF) spectrometer (S4 PIONEER, Bruker AXS, Karlsruhe, Germany).

The amount of $–SO_3$ groups on the surfaces of the prepared catalysts was determined by titration (Jiang, Xu, et al., 2012b). The catalyst (0.1 g) was dispersed in 20 mL of NaCl solution (2 mol/L) and then stirred mechanically for 24 h. The filtrate was titrated with 6 mmol/L of NaOH solution and phenolphthalein was used as an indicator.

Catalytic Performance

The esterification of oleic acid with methanol was used to investigate the catalytic properties of the prepared catalysts. In a typical experiment, 1 g of oleic acid, 8 mL of methanol, and 0.05 g of catalyst were added to a 25 mL three-neck round-bottomed flask equipped with a reflux condenser and a mechanical agitator. The mixture was stirred at 65°C for 4 h. The reaction solution was separated from the mixture using a magnet. The catalyst was recycled by washing with ethanol. The product (0.5 mL) was diluted with 10 mL of *n*-hexane and determined by the GC method (Agilent 6820 GC with a DB-1 capillary column, Agilent Technologies, Santa Clara, California, USA). Heptadecane was used as the internal standard. The catalytic experiment was repeated five times.

Recycling experiments were performed to evaluate the catalyst's stability. At the end of each reaction cycle, the catalyst was recycled using a magnet, washed with ethanol, and dried at 80°C.

Results and Discussion

Preparation and Characterization of Catalyst

XRF analysis of Plg and acid-treated Plg (Table 1) revealed that the component contents of Plg all increased except for CaO, MgO, and MnO after acid treatment. The proportion of CaO (wt.%) decreased visibly from 8.12 to 2.26 wt.%, which suggested that the carbonate minerals existing in Plg were dissolved in the HNO_3 solution. The carbonate mineral in Plg was often dolomite, $CaMg(CO_3)_2$, and so the CaO and MgO contents decreased after the HNO_3 treatment. The loss of MgO was much less than that of CaO, however, because Mg also existed in Plg crystals. The Fe_2O_3 content in Fe_3O_4/Plg increased significantly from 11.33 to 40.01 wt.% after loading of Fe_3O_4 (Table 1) while the amounts of other components decreased. The results indicated that Fe_3O_4 was loaded successfully onto the surface of Plg nanorods, which probably provides the magnetism of the SC-F-Plg catalyst. SO_3 was observed in the acid-treated Plg and

https://doi.org/10.1007/s42860-022-00199-0 Published online by Cambridge University Press

Table 1 Chemical compositions (wt.%) of Plg, acid-treated Plg, and Fe_3O_4/Plg

Sample	Na_2O	Al_2O_3	SiO_2	K_2O	CaO	MnO	TiO_2	Fe_2O_3	MgO	SO_3
Plg	0	10.33	55.81	1.72	8.12	0.19	1.48	10.57	10.40	0
Acid-treated Plg	0	10.48	61.38	1.85	2.26	0.09	1.69	11.33	7.73	1.78
Fe_3O_4/Plg	0.18	6.62	37.37	1.03	1.22	0.42	1.03	40.01	5.32	4.48
SC-F-Plg-3	0.11	5.94	31.63	0.86	1.12	0.19	0.92	31.81	5.23	16.95

Fe_3O_4/Plg, which was derived from the reagents used in the preparation process of acid-treated Plg and Fe_3O_4. A new component of Na_2O appeared in the Fe_3O_4/Plg, which was introduced during the process of forming Fe_3O_4. The amounts of other components were reduced except for SO_3 after the sulfonation and carbonation of Fe_3O_4/Plg, and the amount of SO_3 increased from 4.48 to 16.95%, which suggested that SC existed in the SC-F-Plg catalyst.

The XRD pattern of Plg (Fig. 1a) showed two diffraction peaks at 8.3 and 19.9°2θ, which were ascribed to the characteristic diffraction peaks of Plg (Suárez Barrios et al., 1995). In addition, characteristic diffraction peaks of the quartz impurity (21.2 and 26.5°2θ) also existed in the XRD pattern of Plg after removal of the carbonates using HNO_3 solution (Jiang, Feng, et al., 2012a; Suárez Barrios et al., 1995). No other type of mineral except for quartz was found in the XRD pattern of Plg. A weak and broad diffraction peak from 15 to 30°2θ was observed in the SC patterns (Jiang, Xu, et al., 2012b), suggesting the presence of an amorphous carbon material (Fig. 1b). The intensities of the diffraction peaks of Plg and quartz were significantly reduced after

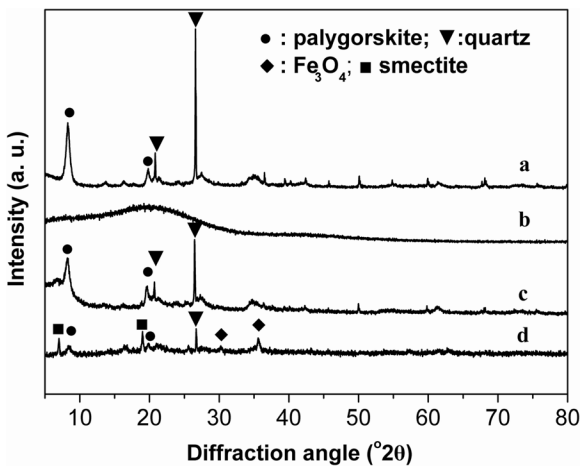


Fig. 1 XRD patterns of **a** Plg, **b** SC, **c** SC-Plg-3, and **d** SC-F-Plg-3

sucrose carbonization, which may be due to the loading of amorphous carbon materials (Fig. 1c). Their intensities were further reduced after loading of Fe_3O_4 and subsequent carbonization of sucrose (Fig. 1d). The characteristic diffraction peaks located at 30.2 and 35.5°2θ were observed in the XRD pattern of SC-F-Plg, indicating the presence of Fe_3O_4 in the catalyst (Bae et al., 1998). In addition, two weak diffraction peaks at 6.9 and 18.9°2θ, ascribed to smectite (Golden & Dixon, 1990; Whitney, 1990), could be observed in the XRD pattern of SC-Plg-3. Two diffraction peaks of smectite at 6.9 and 18.9°2θ were also present in the XRD pattern of SC-F-Plg-3 and their peak intensities were greatly increased after the introduction of Fe_3O_4. The intensity of the diffraction peak of smectite at 6.9°2θ varied significantly with acidity (Cui et al., 2020). The diffraction peak of smectite broadened gradually with increase in the pH and its intensity was greatest at pH = 1 because smectite was gradually disordered with increasing pH value (Cui et al., 2020). In addtion, due to the introduction of Fe_3O_4 nanoparticles into the interlamellar spaces of smectite, the disordered-layers structure of smectite was reorganized to the ordered-layers, resulting in the appearance of a (001) diffraction peak (Zeynizadeh et al., 2020). Therefore, smectite may have existed in the original Plg in this study, and then the iron species and high acidity collectively promoted the disordered-layers structure of smectite to the ordered-layers, which caused the appearance of the diffraction peaks of smectite. The results also illustrated that sucrose carbonization at 200°C did not change the Fe_3O_4 phase, which determined the magnetic property of the catalyst.

The SEM image of Plg showed that Plg possessed typical rod-like morphology (Fig. 2a). Sulfonated carbon comprised solid particles with a smoother surface (Fig. 2b) (Jiang, Xu, et al., 2012b). The spaces between Plg nanorods were filled by carbon material and the surface of the SC-Plg-3 was smoother than that of Plg though dispersed Plg nanorods were clearly observed in SC-Plg-3 (Fig. 2c), indicating that carbon material was

https://doi.org/10.1007/s42860-022-00199-0 Published online by Cambridge University Press

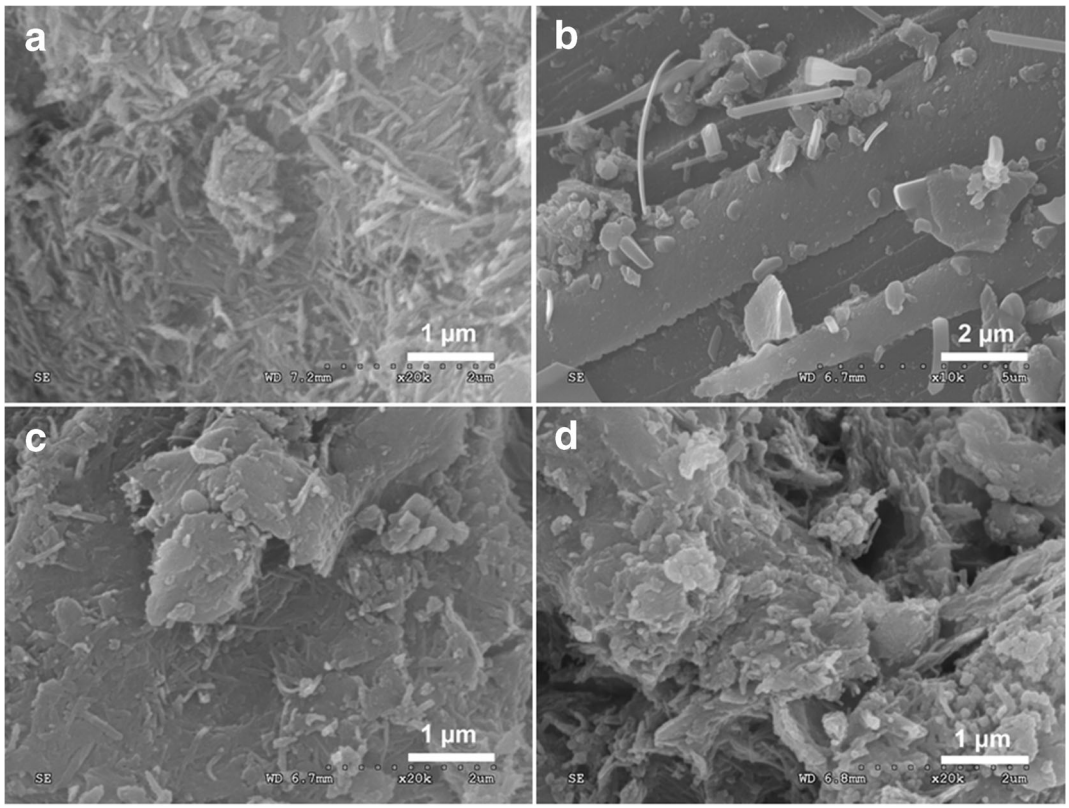


Fig. 2 SEM images of **a** Plg, **b** SC, **c** SC-Plg-3, and **d** SC-F-Plg-3

formed on the surface of Plg nanorods after sucrose carbonization. The morphology of SC-F-Plg-3 was similar to that of the SC-Plg-3, though some solid particles appeared in the SC-F-Plg-3 (Fig. 2d), which correspond to Fe_3O_4 nanoparticles according to XRD analysis.

The TEM image of Plg crystals displayed a rod-shaped morphology with lengths of 10–30 nm (Fig. 3a). Some nanosized spherical particles, ascribed to quartz, were attached to these Plg nanorods (Jiang et al., 2014). The Plg nanorods and spherical nanoparticles were wrapped in carbon materials after sucrose carbonization (Fig. 3b). The TEM images of SC-F-Plg-3 (Fig. 3c) revealed the appearance of numerous nanoparticles on the Plg surfaces, which was a mixture of SC and Plg nanorods. The magnified TEM images of SC-F-Plg-3 (Fig. 3d) further indicated that these nanoparticles were loaded on rod-shaped Plg crystals and then were coated with a carbon nanolayer. The black nanoparticles were identified as Fe_3O_4 according to the XRD analysis results of SC-F-Plg-3.

The EDX spectra of Plg revealed that silicon (Si), magnesium (Mg), aluminum (Al), iron (Fe), and oxygen (O) were the major elements of Plg (Fig. 4), while trace carbon was also present (Zhang et al., 2020). As shown by the EDX spectra of Plg and SC-F-Plg-3, the peak intensities of Si, Mg, Al, and O decreased after loading of Fe_3O_4 and sucrose carbonization. Furthermore, the peak intensities of Fe and carbon increased significantly. Sulfur derived from TsOH appeared in the EDX spectrum of SC-F-Plg-3. The TEM-EDX images of SC-F-Plg-3 indicated that O, Si, and Fe were distributed uniformly in the same area of SC-F-Plg-3 (Fig. 4). The distribution densities of O and Si were much greater than that of Fe because O and Si were the main elements in Plg. However, the distribution of S in SC-F-Plg-3 was relatively sparse compared to these elements derived from Plg. Note that the distribution densities of Fe and S were close to that of Si in the left section of the SC-F-Plg-3 nanorod, which illustrated the presence of Fe_3O_4 and sulfonated carbon. The results further indicated that Fe_3O_4 and sulfur-containing carbon material were loaded onto the surface of the Plg nanorods.

The FTIR spectra of Plg and SC-F-Plg-3 were used to identify the presence of $–SO_3H$ groups (Fig. 5). Compared to Plg, five new bands at 1008, 1040, 1125, 1380, and 1620 cm^{-1} were observed in the FTIR spectrum of

https://doi.org/10.1007/s42860-022-00199-0 Published online by Cambridge University Press

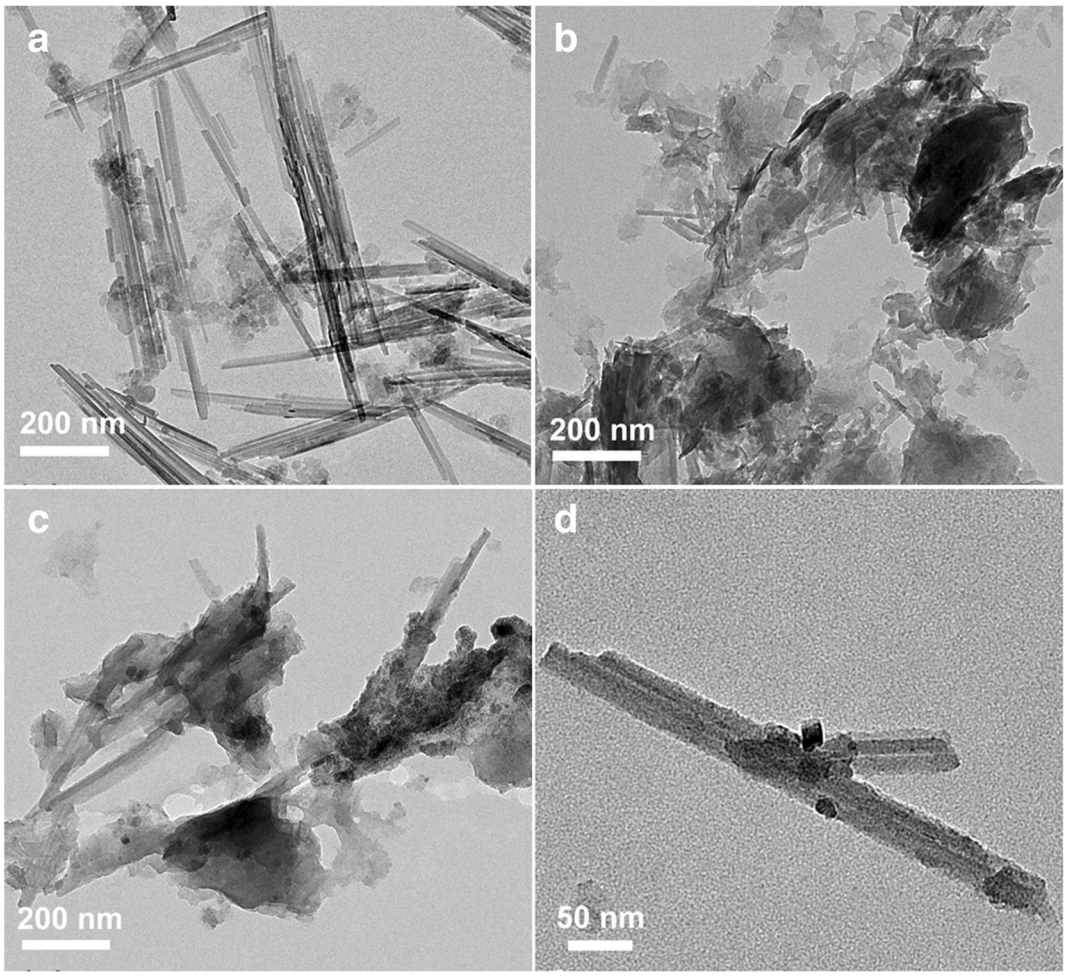


Fig. 3 TEM images of **a** Plg, **b** SC, **c** SC-Plg-3, and **d** SC-F-Plg-3

SC-F-Plg-3 (Fig. 5). The vibrational bands at 1008 and 1040 cm^{-1} corresponded to S=O asymmetric stretching of $–SO_3H$ groups (Geng et al., 2011; Iroh & Williams, 1999), while the bands at 1125 and 1380 cm^{-1} corresponded to the asymmetric SO_2 stretching of $–SO_3H$ groups (Geng et al., 2011; Peng et al., 2010). The band at 1620 cm^{-1} is related to C=C skeletal vibrations (Laohapornchaiphan et al., 2017; Xiao et al., 2010). These results showed that $–SO_3H$ groups were introduced into the carbonaceous material via the addition of TsOH.

The S 2p XPS spectrum of SC-F-Plg-3 (Fig. 6a) revealed a single S 2p peak at 168 eV, which further indicated that all S atoms of SC-F-Plg-3 were in the form of the $–SO_3H$ groups (Suganuma et al., 2010; Zhan et al., 2014). As shown in the Fe 2p XPS spectrum of SC-F-Plg-3 (Fig. 6b), the two peaks observed at 710 and 724 eV corresponded to Fe $2p_{3/2}$ and Fe $2p_{1/2}$, which confirmed the presence of Fe_3O_4 (Yamashita & Hayes, 2008). The results further illustrated that the primary acid groups and magnetic material of SC-F-Plg-3 were $–SO_3H$ group and Fe_3O_4, respectively.

The SEM images of SC-F-Plg prepared using various sucrose dosages revealed that the space between Fe_3O_4 nanoparticles and Plg nanorods filled gradually with increasing amounts of sucrose (Fig. 7).The rod-shaped morphology of Plg crystals was still observed in SC-F-Plg catalysts, however. The corresponding XRD patterns all revealed the presence of smectite, an Fe_3O_4 phase, and Plg crystals, while the intensity of these characteristic diffraction peaks was not reduced (Fig. 8), although the sucrose dosage increased. The results indicated that the carbon layer on the surface of Fe_3O_4 nanoparticles and Plg nanorods was very thin, in agreement with the TEM image of SC-F-Plg-3 (Fig. 3).

https://doi.org/10.1007/s42860-022-00199-0 Published online by Cambridge University Press

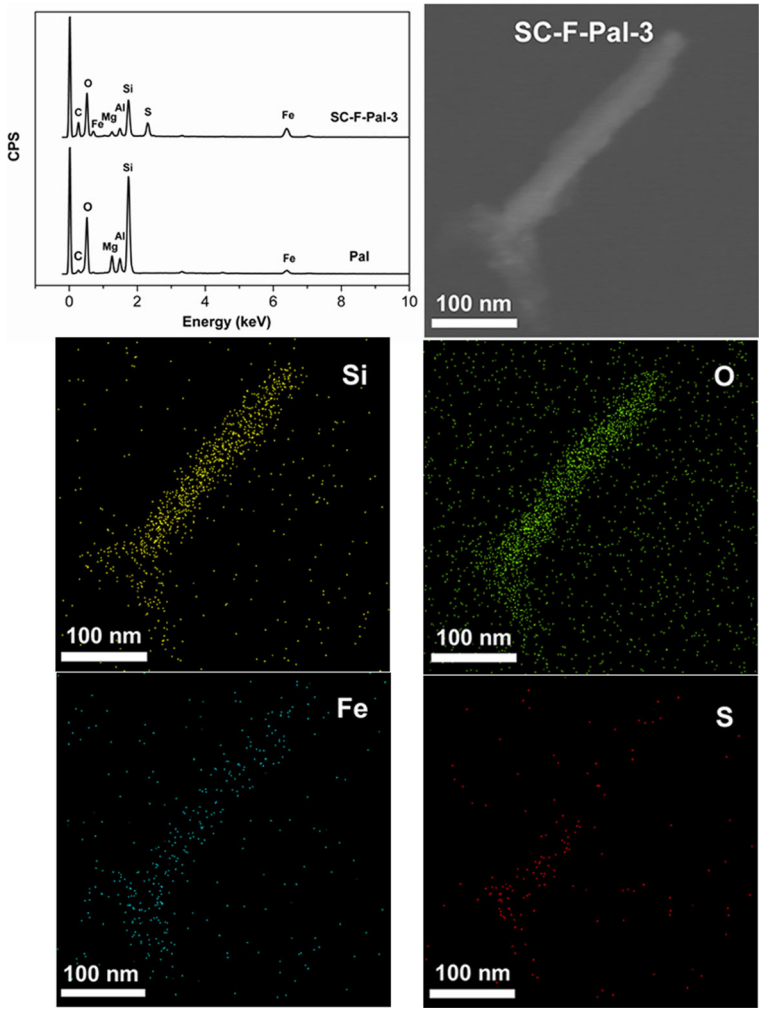


Fig. 4 EDX spectra of Plg and SC-F-Plg-3 and TEM-EDX element mapping images of SC-F-Plg-3

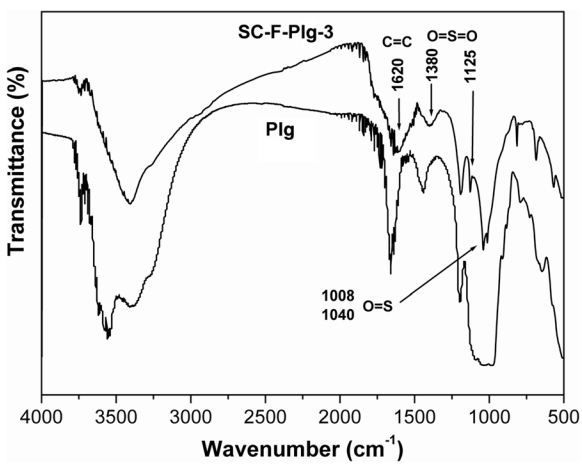


Fig. 5 FTIR spectra of Plg and SC-F-Plg-3

The magnetic performance of SC-F-Plg was derived from Fe_3O_4 nanoparticles. The XRF analysis results of Fe_3O_4/Plg (Table 1) revealed that the loading of Fe_3O_4 was ~27.7 wt.% while the amount of Plg was 72.3 wt.%. The saturation magnetization (M_S) value of Fe_3O_4/Plg was measured to be 20.82 emu/g. Hence, the M_S value of Fe_3O_4 was calculated as 75.18 emu/g. The M_S values of SC-F-Plg were 5.28, 5.21, 4.96, and 4.67 emu/g with increasing sucrose dosage (Table 2). The corresponding Fe_3O_4 amounts were 6.97, 6.93, 6.59, and 6.21 wt.%, respectively. The magnetic curve of SC-F-Plg-3 exhibited ferromagnetic behavior and the M_S value was 5.21 emu/g (Fig. 9), indicating that SC-F-Plg-3 possessed an excellent magnetic property, which was greater than the saturation magnetization of ATP/C@NiFe-LDH (2.01 emu/g) (Tang et al., 2018). Furthermore, SC-F-Plg-3 was removed easily from the

https://doi.org/10.1007/s42860-022-00199-0 Published online by Cambridge University Press

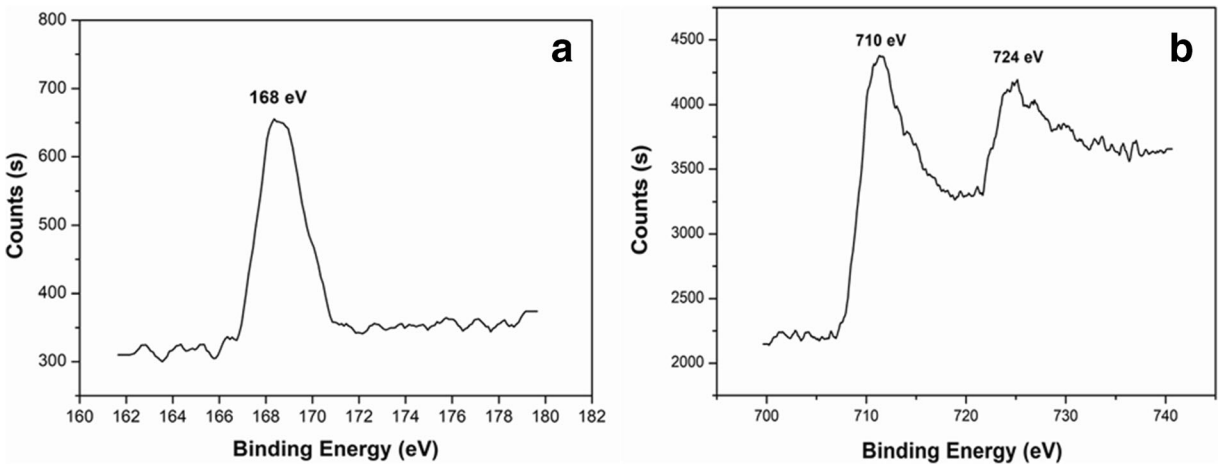


Fig. 6 **a** S 2p and **b** Fe 2p XPS spectra of SC-F-Plg-3

liquid reaction system under an external magnetic field after the reaction. The saturation magnetization value of the recycled SC-F-Plg-3 was reduced slightly to 5.15 emg/g after five cycles, indicating that the magnetic property of SC-F-Plg-3 was very stable. The results further confirmed that Fe_3O_4 nanoparticles were wrapped in carbon material, which protected them from oxidation and fall-out from the catalyst.

The textural properties of Plg, SC, SC-Plg-3, and SC-F-Plg catalysts were compared (Table 3). The BET surface area and pore volume of Plg were 169 m^2/g and 0.324 cm^3/g, respectively. Owing to its non-porous

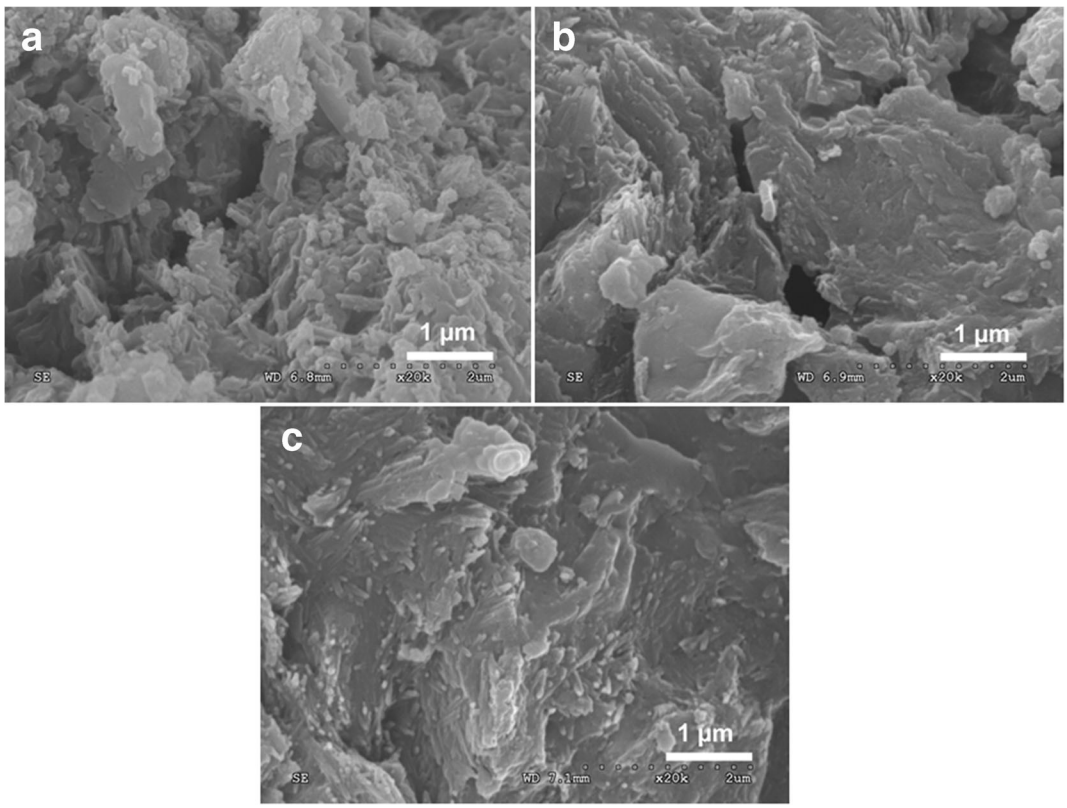


Fig. 7 SEM images of **a** SC-F-Plg-1, **b** SC-F-Plg-5, and **c** SC-F-Plg-7

https://doi.org/10.1007/s42860-022-00199-0 Published online by Cambridge University Press

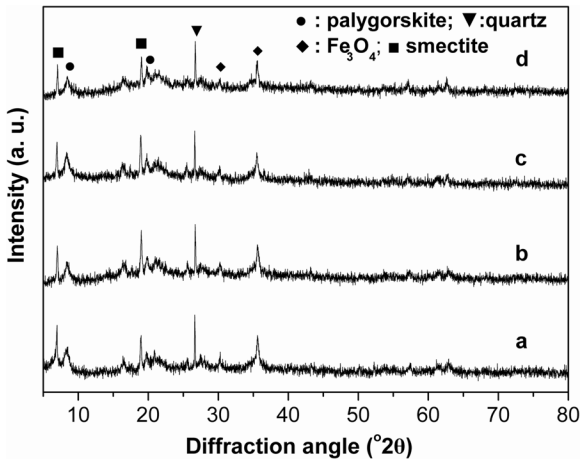


Fig. 8 XRD patterns of **a** SC-F-Plg-1, **b** SC-F-Plg-3, **c** SC-F-Plg-5, and **d** SC-F-Plg-7

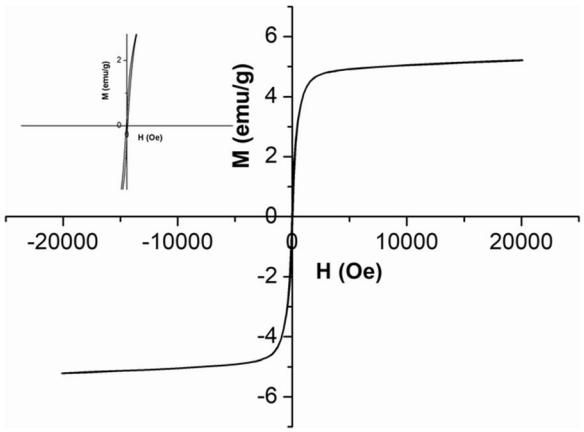


Fig. 9 Magnetic hysteresis loop of SC-F-Plg-3

structure, the BET surface area and pore volume of SC were not recorded. The BET surface area and pore volume of SC-Plg-3 increased to 62 m^2/g and 0.162 cm^3/g, respectively, due to the introduction of Plg nanorods with a porous structure and the dispersion of SC particles on the Plg surfaces. Compared to SC-Plg-3, the BET surface area and pore volume of SC-F-Plg decreased in the presence of Fe_3O_4 nanoparticles. The BET surface area and pore volume of SC-F-Plg further decreased with increasing amount of sucrose, which were approximately zero when the dosage of sucrose was 7 g. The results indicated that carbon was deposited successfully in the mesopores of Plg and on the external Plg surfaces and Fe_3O_4 nanoparticles, which decreased the BET surface area and pore volume of the catalysts.The BET surface area of SC increased, however, during the loading of Plg and Fe_3O_4 nanoparticles.

Elemental analysis of SC and SC-F-Plg (Table 2) revealed the presence of sulfur, hydrogen, nitrogen, and carbon derived from sucrose and TsOH. The SC contained the most carbon and sulfur (3.420 wt.%). The sulfur and carbon contents of SC-Plg-3 decreased significantly after the introduction of Plg nanorods. The sulfur content of SC-F-Plg-1 (2.400 wt.%) was greater than that of SC-Plg-3 (1.656 wt.%) despite reducing carbon materials. SC-F-Plg-3 also contained more carbon and sulfur than SC-Plg-3. The sulfonation reaction appeared to occur at the interface between carbon materials and TsOH. This phenomenon may be caused by dispersed Fe_3O_4 nanoparticles which favored the deposition and dispersion of carbon material compared with Plg nanorods, increasing sulfur and carbon contents. The results indicated that the carbon layer on the surfaces of Fe_3O_4 nanoparticles and Plg may thicken with increasing sucrose dosage, which may hinder the sulfonation reaction. Thus, SC-F-Plg's carbon, hydrogen, and nitrogen contents increased with increasing sucrose dosage, whereas its sulfur content decreased gradually.

Table 2 Elemental analysis of SC and SC-F-Plg (wt.%) and magnetic performance of SC-F-Plg

Catalyst	C	H	N	S	M_s (emu/g)
SC	65.64	7.013	0.328	3.420	—
SC-Plg-3	16.86	1.832	0.122	1.656	—
SC-F-Plg-1	10.45	2.353	0.126	2.400	5.28
SC-F-Plg-3	17.41	2.860	0.132	2.202	5.21
SC-F-Plg-5	24.33	3.818	0.155	1.881	4.96
SC-F-Plg-7	30.19	4.615	0.193	1.824	4.67
R-SC-F-Plg-3	11.63	1.259	0.172	0.352	5.15

The catalytic properties of carbon-based solid acid catalysts are usually determined by their free acid groups (Ngaosuwan et al., 2016). The numbers of acidic –SO_3H groups on the surface of the catalysts were obtained by neutralization titration with NaOH (Table 3). By comparison, the units for sulfur content (wt.%) were converted to mmol/g and listed in Table 3. The acid content of SC was 0.345 mmol/g and this was due to greater sulfur content (1.070 mmol/g), indicating that SC possessed abundant surface –SO_3H groups and some sulfur atoms were sealed within the carbon materials. Compared to SC, the Plg was weakly acidic (Araújo Melo et al., 2002). The acid content in SC-Plg-3 decreased from 0.345 to 0.024 mmol/g after the introduction of Plg.

On the contrary, the acid content of SC-F-Plg-1 increased to 0.060 mmol/g after the addition of Fe_3O_4

https://doi.org/10.1007/s42860-022-00199-0 Published online by Cambridge University Press

Table 3 Textural properties, composition analysis, acid density, and catalytic properties of catalysts

Catalyst	BET surface area (m^2/g)	Pore volume (cm^3/g)	Acid content of –SO_3H (mmol/g)	S content (mmol/g)	Conversion [a] (%)
—	—	—	—	—	50.37
Plg	169	0.324	—	—	65.07
SC	—	—	0.345	1.070	88.87
SC-Plg-3	62	0.162	0.024	0.518	82.79
SC-F-Plg-1	36.6	0.127	0.060	0.750	80.84
SC-F-Plg-3	8.4	0.027	0.087	0.688	88.69
SC-F-Plg-5	0.42	0.003	0.087	0.588	84.43
SC-F-Plg-7	0.002	0.001	0.048	0.587	84.17

[a] conversion of oleic acid

nanoparticles, which further illustrated that Fe_3O_4 nanoparticles may benefit the dispersion of carbon material compared with Plg. These dispersed carbon materials contributed to the loading and release of –SO_3H groups. The acid content of SC-F-Plg increased slowly with sucrose but decreased at a sucrose dosage of 7 g. The results indicated that the increase in layer thickness of the carbon on the surfaces of Fe_3O_4 nanoparticles and Plg may inhibit the release of –SO_3H groups. Hence, the acid content of SC-F-Plg increased first and then decreased. Therefore, the dispersed and thin carbon layer on the surface of Fe_3O_4 nanoparticles benefited the free –SO_3H group despite the relatively small sulfur content, which meant that the catalyst had greater catalytic properties.

Catalytic Performance of Catalyst

The esterification of oleic acid with methanol was used to evaluate the catalytic activity of SC-F-Plg (Table 3). The conversion of oleic acid was 50.37% in the absence of a catalyst but increased to 65.07% after the addition of the Plg catalyst. Because of a few acid sites in Plg, the improvement in conversion of oleic acid was only slight (Araújo Melo et al., 2002). The –SO_3H groups on the surface of SC promoted the esterification of oleic acid with methanol. The SC improved oleic acid conversion to 88.87% for a larger amount of acid, therefore. Compared to SC, the introduction of Plg maintained a conversion rate of 82.79% due to larger surface area of SC-Plg-3 despite a very small amount of acid, which increased the contact of reactants with catalytic sites and subsequently enhanced the catalytic efficiency. The conversion of oleic acid over SC-F-Plg-3 increased to 88.69% even though a significant loss of surface area was observed with the introduction of Fe_3O_4 nanoparticles to SC-Plg-3 catalyst. Although this catalyst had a larger surface area, oleic acid conversion over SC-F-Plg-1 showed a slight decline and was 80.84%, which stemmed from the reduced acid content when the amount of sucrose was decreased from 3 to 1 g. The loss of surface area or acid content promoted reduction of oleic acid conversion on SC-F-Plg with increasing sucrose dosage from 5 to 7 g. Hence, SC-F-Plg possessed excellent catalytic properties, owing to the surface area and acid content of the catalyst. The role of Plg nanorods was, thus, primarily as a porous carrier of SC and it increased the surface area of the catalyst despite

Table 4 Comparison of esterification of oleic acid with methanol over various catalysts

Catalysts	Sulfonating agent	Catalyst dosage (g/g acid)	Alcohol/acid (molar ratio)	Temperature (°C)	Time (h)	Conversion [a] (%)
Mesoporous SO_3H–carbon	H_2SO_4	0.07	10	80	10	58 (Peng et al., 2010)
SBA-15-C-SO_3H	TsOH-H_2SO_4	0.036	10	80	5	85.2 (Wang et al., 2015)
SC-F-Plg-3	TsOH	0.02	55	65	4	88.69
Sulfonated carbon	H_2SO_4	0.1	20	65	6	90 (Flores et al., 2019)

[a] Conversion of oleic acid

https://doi.org/10.1007/s42860-022-00199-0 Published online by Cambridge University Press

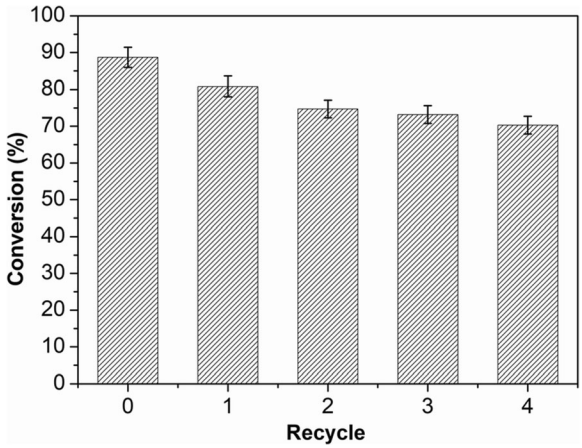


Fig. 10 Reusability of SC-F-Plg-3

fewer acid sites on Plg. On the other hand, Plg also contributed to the dispersion of Fe_3O_4 nanoparticles. The carbon layer was uniform and thin, which was well suited to the introduction of Fe_3O_4 nanoparticles and Plg nanorods, resulting in the increased acid content and catalytic properties of SC-F-Plg.

The catalytic activities of various sulfonated carbon catalysts were compared using the esterification of oleic acid with methanol (Table 4). The conversion of oleic acid over SC-F-Plg-3 was greater than that of mesoporous SO_3H-carbon and SBA-15-C-SO_3H prepared using sulfuric acid as the sulfonating agent despite the higher reaction temperature used for the latter catalysts (Peng et al., 2010; Wang et al., 2015). Oleic acid conversion was slightly lower than sulfonated carbon (90%) (Flores et al., 2019). The results illustrated that natural clay Plg could replace expensive SBA-15 mesoporous molecular sieves as a catalyst carrier.

The catalyst stability and reusability were tested using the SC-F-Plg-3 sample. The SC-F-Plg-3 catalyst led to oleic-acid conversion of up to 70.31% after the fifth cycle (Fig. 10). This was greater than the recycled sugarcane bagasse-derived sulfonated carbon (66.6%) (Flores et al., 2019). The results indicated that SC-F-Plg-3 possessed good catalytic activity and stability. Its sulfur content decreased from 2.202 to 0.352 wt.% after the fifth cycle (Table 2). The carbon content of the recycled SC-F-Plg-3 (R-SC-F-Plg-3) also decreased to 11.48 wt.% (Table 2), indicating loss of carbon material from SC-F-Plg-3 catalyst during the reaction process. The decreased catalytic activity of SC-F-Plg-3 may be attributed primarily to the loss of –SO_3H groups from the carbonaceous material (Jiang, Xu, et al., 2012b). On the other hand, a small loss of SC from the catalyst also led to diminished catalytic activity of the SC-F-Plg-3.

Conclusions

The SC-F-Plg catalyst was prepared from a mixture of sucrose, TsOH, and Fe_3O_4/Plg in an environmentally friendly and low-cost approach. Plg nanorods were mainly used as the carriers to replace sucrose-derived carbon, to disperse Fe_3O_4 nanoparticles, and to increase the surface area of the catalyst. The introduction of Fe_3O_4 nanoparticles provided the catalyst with suitable magnetism, which helped with the formation of a uniform and thin carbon layer on the catalyst's surface, resulting in a larger acid content in the SC-F-Plg. The SC-F-Plg possessed good catalytic activity and stability. The magnetic property of SC-F-Plg was also stable for the protection of Fe_3O_4 nanoparticles in the carbon material. Hence, SC-F-Plg is a promising, cost-effective, and easily-recyclable, carbon-based solid acid composite catalyst.

Acknowledgments This work was supported by the Six Talent Peaks Project in Jiangsu Province (No. 2018-JNHB-009), Natural Science Key Project of the Jiangsu Higher Education Institutions (19KJA430015), the Foundation of Key Laboratory for Palygorskite Science and Applied Technology of Jiangsu Province (HPZ202001), and the National & Local Joint Engineering Research Center for Mineral Salt Deep Utilization (SF201906, SF202103). The first author is grateful to Dr Nisar Ali for his help in completing the paper.

Code Availability Not Applicable.

Authors' Contributions All authors contributed to the study conception and design. Material preparation, data collection and analysis were performed by Mei Wu, Xingjun Yao, Jing Ouyang and Jinlong Jiang. All authors read and approved the final manuscript.

Funding Funding sources are as stated in the Acknowledgements.

Data Availability All data generated or analysed during this study are included in the manuscript.

Declarations

Conflict of Interest The authors declare that they have no conflict of interest.

Ethics Approval Not Applicable.

https://doi.org/10.1007/s42860-022-00199-0 Published online by Cambridge University Press

Consent to Participate Not Applicable.

Consent for Publication Not Applicable.

References

Araújo Melo, D. M., Ruiz, J. A. C., Melo, M. A. F., Sobrinbo, E. V., & Martinelli, A. E. (2002). Preparation and characterization of lanthanum palygorskite clays as acid catalysts. *Journal of Alloys and Compounds, 344*, 352–355.

Bae, D. S., Han, K. S., Cho, S. B., & Choi, S. H. (1998). Synthesis of ultrafine Fe_3O_4 powder by glycothermal process. *Materials Letters, 37*, 255–258.

Ballotin, F. C., da Silva, M. J., Lago, R. M., & de Carvalho Teixeir, A. P. (2020). Solid acid catalysts based on sulfonated carbon nanostructures embedded in an amorphous matrix produced from bio-oil: esterification of oleic acid with methanol. *Journal of Environmental Chemical Engineering, 8*, 103674.

Cui, J., Zhang, Z., & Han, F. (2020). Effects of pH on the gel properties of montmorillonite, palygorskite and montmorillonite-palygorskite composite clay. *Applied Clay Science, 190*, 105543.

Dehkhoda, A. M., West, A. H., & Ellis, N. (2010). Biochar based solid acid catalyst for biodiesel production. *Applied Catalysis A: General, 382*, 197–204.

Flores, K. P., Omega, J. L. O., Cabatingan, L. K., Go, A. W., Agapay, R. C., & Ju, Y. H. (2019). Simultaneously carbonized and sulfonated sugarcane bagasse as solid acid catalyst for the esterification of oleic acid with methanol. *Renewable Energy, 130*, 510–523.

Geng, L., Wang, Y., Yu, G., & Zhu, Y. (2011). Efficient carbon-based solid acid catalysts for the esterification of oleic acid. *Catalysis Communications, 13*, 26–30.

Golden, D. C., & Dixon, J. B. (1990). Low-temperature alteration of palygorskite to smectite. *Clays and Clay Minerals, 38*, 401–408.

Iroh, J. O., & Williams, C. (1999). Formation of thermally stable polypyrrole-naphthalener/benzene sulfonate-carbon fiber composites by an electrochemical process. *Synthetic Metals, 99*, 1–8.

Jiang, J., Feng, L., Gu, X., Qian, Y., Gu, Y., & Duanmu, C. S. (2012a). Synthesis of zeolite A from palygorskite via acid activation. *Applied Clay Science, 55*, 108–113.

Jiang, J., Xu, Y., Duanmu, C. S., Gu, X., & Chen, J. (2012b). Preparation and catalytic properties of sulfonated carbon-palygorskite solid acid catalyst. *Applied Clay Science, 95*, 260–264.

Jiang, J., Chen, Z., Duanmu, C. S., Gu, Y., Chen, J., & Ni, L. (2014). Economical synthesis of amorphous carbon nanotubes and SBA-15 mesoporous materials using palygorskite as a template and silica source. *Materials Letters, 132*, 425–427.

Kasprzak, A., Bystrzejewski, M., & Poplawska, M. (2018). Sulfonated carbon-encapsulated iron nanoparticles as an efficient magnetic nanocatalyst for highly selective synthesis of benzimidazoles. *Dalton Transactions, 47*, 6314–6322.

Konwar, L. J., Das, R., Thakur, A. J., Salminen, E., Mäki-Arvela, P., Kumar, N., Mikkola, J. P., & Deka, D. (2014). Biodiesel production from acid oils using sulfonated carbon catalyst derived from oil-cake waste. *Journal of Molecular Catalysis A: Chemical, 388–389*, 167–176.

Laohapornchaiphan, J., Smith, C. B., & Smith, S. M. (2017). One-step preparation of carbon-based solid acid catalyst from water hyacinth leaves for esterification of oleic acid and dehydration of xylose. *Chemistry – An Asian Journal, 12*, 3178–3186.

Mansoori, Z., & Mansoori, Y. (2018). Fe_3O_4@SiO_2-SO_3H Nanoparticles: An efficient magnetically retrievable catalyst for esterification reactions. *Journal of Particle Science Technology, 4*, 67–79.

Middea, A., Spinelli, L. S., Souza Junior, F. G., Neumann, R., da FM Gomes, O., Fernandes, T. L. A. P., de Lima, L. C., Barthem, V. M. T. S., & de Carvalho, F. V. (2015). Synthesis and characterization of magnetic palygorskite nanoparticles and their application on methylene blue remotion from water. *Applied Surface Science, 346*, 232–239.

Murray, H. H. (2000). Traditional and new applications for kaolin, smectite, and palygorskite: a general overview. *Applied Clay Science, 17*, 207–221.

Ngaosuwan, K., Goodwin Jr., J. G., & Prasertdham, P. (2016). A green sulfonated carbon-based catalyst derived from coffee residue for esterification. *Renewable Energy, 86*, 262–269.

Palani, A., & Pandurangan, A. (2005). Esterification of acetic acid over mesoporous Al-MCM-41 molecular sieves. *Journal of Molecular Catalysis A: Chemical, 226*, 129–226134.

Peng, L., Philippaerts, A., Ke, X., Noyen, J. V., Clippel, F. D., Tendeloo, G. V., Jacobs, P. A., & Sels, B. F. (2010). Preparation of sulfonated ordered mesoporous carbon and its use for the esterification of fatty acids. *Catalysis Today, 150*, 140–146.

Pileidis, F. D., Tabassum, M., Coutts, S., & Ttitirici, M. M. (2014). Esterification of levulinic acid into ethyl levulinate catalysed by sulfonated hydrothermal carbons. *Chinese Journal of Catalysis, 35*, 929–936.

Polshettiwar, V., Luque, R., Fihri, A., Zhu, H., Bouhrara, M., & Basset, J. M. (2011). Magnetically Recoverable Nanocatalysts. *Chemical Reviews, 111*, 3036–3075.

Rao, B. V. S. K., Chandra Mouli, K., Rambabu, N., Dalai, A. K., & Prasad, R. B. N. (2011). Carbon-based solid acid catalyst from de-oiled canola meal for biodiesel production. *Catalysis Communications, 14*, 20–26.

Sarkar, B., Liu, E., McClure, S., Sundaramurthy, J., Srinivasan, M., & Naidu, R. (2015). Biomass derived palygorskite-carbon nanocomposites: Synthesis, characterisation and affinity to dye compounds. *Applied Clay Science, 114*, 617–626.

Sejidov, F. T., Mansoori, Y., & Goodarzi, N. (2005). Esterification reaction using solid heterogeneous acid catalysts under solvent-less condition. *Journal of Molecular Catalysis A: Chemical, 204*, 186–190.

Shu, Q., Gao, J., Nawaz, Z., Liao, Y., Wang, D., & Wang, J. (2010). Synthesis of biodiesel from waste vegetable oil with large amounts of free fatty acids using a carbon-based solid acid catalyst. *Applied Energy, 87*, 2589–2596.

https://doi.org/10.1007/s42860-022-00199-0 Published online by Cambridge University Press

Suárez Barrios, M., Flores González, L. V., Vicente Rodríguez, M. A., & Martín Pozas, J. M. (1995). Acid activation of a palygorskite with HCl: development of physico-chemical, textural and surface properties. *Applied Clay Science, 10*, 247–258.

Suganuma, S., Nakajima, K., Kitano, M., Yamaguchi, D., Kato, H., Hayashi, S., & Hara, M. (2010). Synthesis and acid catalysis of cellulose-derived carbon-based solid acid. *Solid State Sciences, 12*, 1029–1024.

Tang, J., Mu, B., Zong, L., Zheng, M., & Wang, A. (2017). Facile and green fabrication of magnetically recyclable carboxyl-functionalized attapulgite/carbon nanocomposites derived from spent bleaching earth for wastewater treatment. *Chemical Engineering Journal, 322*, 102–114.

Tang, J., Mu, B., Zong, L., & Wang, A. (2018). One-step synthesis of magnetic attapulgite/carbon supported NiFe-LDHs by hydrothermal process of spent bleaching earth for pollutants removal. *Journal of Cleaner Production, 172*, 673–685.

Testa, M. L., Parola, V. L., & Venezia, A. M. (2010). Esterification of acetic acid with butanol over sulfonic acid-functionalized hybrid silicas. *Catalysis Today, 158*, 109–113.

Toda, M., Takagaki, A., Okamura, M., Kondo, J. N., Hayashi, S., Domen, K., & Hara, M. (2005). Biodiesel made with sugar catalyst. *Nature, 438*, 178.

Van de Vyver, S., Peng, L., Geboers, J., Schepers, H., de Clippel, F., Gommes, C. J., Goderis, B., Jacobs, P. A., & Sels, B. F. (2010). Sulfonated silica/carbon nanocomposites as novel catalysts for hydrolysis of cellulose to glucose. *Green Chemistry, 12*, 1560–1563.

Wang, J., Xu, W., Ren, J., Liu, X., Lu, G., & Wang, Y. (2011). Efficient catalytic conversion of fructose into hydroxymethylfurfural by a novel carbon-based solid acid. *Green Chemistry, 13*, 2678–2681.

Wang, Y., Wang, D., Tan, M., Jiang, B., Zheng, J., Tsubaki, N., & Wu, M. (2015). Monodispersed hollow SO_3H-functionalized carbon/silica as efficient solid acid catalyst for esterification of oleic acid. *ACS Applied Materials & Interfaces, 7*, 26767–26775.

Wang, Y. T., Yang, X. X., Xu, J., Wang, H. L., Wang, Z. B., Zhang, L., Wang, S. L., & Liang, J. L. (2019). Biodiesel production from esterification of oleic acid by a sulfonated magnetic solid acid catalyst. *Renewable Energy, 139*, 688–695.

Whitney, G. (1990). Role of water in the smectite-to-illite reaction. *Clay and Clay Minerals, 38*, 343–350.

Xiao, H., Guo, Y., & Liang, X. (2010). One-step synthesis of a novel carbon-based strong acid catalyst through hydrothermal carbonization. *Monatshefte für Chemie, 141*, 929–932.

Xie, W., & Wang, H. (2021). Grafting copolymerization of dual acidic ionic liquid on core-shell structured magnetic silica: A magnetically recyclable Brönsted acid catalyst for biodiesel production by one-pot transformation of low-quality oils. *Fuel, 283*, 118893.

Xie, W., Han, Y., & Wang, H. (2018). Magnetic Fe_3O_4/MCM-41 composite-supported sodium silicate as heterogeneous catalysts for biodiesel production. *Renewable Energy, 125*, 675–681.

Yamashita, T., & Hayes, P. (2008). Analysis of XPS spectra of Fe^{2+} and Fe^{3+} ions in oxide materials. *Applied Surface Science, 254*, 2441–2449.

Yang, J., Ao, Z., Wu, H., Zhang, S., Chi, C., Hou, C., & Qian, W. (2020). Waste paper-derived magnetic carbon composite: A novel eco-friendly solid acid for the synthesis of n-butyl levulinate from furfuryl alcohol. *Renewable Energy, 146*, 477–483.

Zeynizadeh, B., Rahmani, S., & Tizhoush, H. (2020). The immobilized Cu nanoparticles on magnetic montmorillonite (MMT@Fe_3O_4@Cu): As an efficient and reusable nanocatalyst for reduction and reductive-acetylation of nitroarenes with $NaBH_4$. *Polyhedron, 175*, 114201.

Zhan, S., Tao, X., Cai, L., Liu, X., & Liu, T. (2014). The carbon material functionalized with NH_2^+ and SO_3H groups catalyzed esterification with high activity and selectivity. *Green Chemistry, 16*, 4649–4653.

Zhang, S., Zhong, L., Yang, H., Tang, A., & Zuo, X. (2020). Magnetic carbon-coated palygorskite loaded with cobalt nanoparticles for Congo Red removal from waters. *Applied Clay Science, 198*, 105856.

Zhang, J., Jiang, W., Jiang, J., Wu, M., Shi, Y., Mao, P., & Deng, Q. (2021). One-step synthesis of sulfonated carbon/palygorskite solid-acid catalyst for the esterification of oleic acid with methanol. *Clay and Clay Minerals, 69*, 389–396.

Springer Nature or its licensor holds exclusive rights to this article under a publishing agreement with the author(s) or other rightsholder(s); author self-archiving of the accepted manuscript version of this article is solely governed by the terms of such publishing agreement and applicable law.

https://doi.org/10.1007/s42860-022-00199-0 Published online by Cambridge University Press